We are IntechOpen, the world's leading publisher of Open Access books Built by scientists, for scientists

4,800
Open access books available

122,000
International authors and editors

135M
Downloads

Our authors are among the

154
Countries delivered to

TOP 1%
most cited scientists

12.2%
Contributors from top 500 universities

CLARIVATE ANALYTICS BOOK CITATION INDEX INDEXED

WEB OF SCIENCE™

Selection of our books indexed in the Book Citation Index in Web of Science™ Core Collection (BKCI)

Interested in publishing with us?
Contact book.department@intechopen.com

Numbers displayed above are based on latest data collected.
For more information visit www.intechopen.com

17

Cell Biometrics Based on Bio-Impedance Measurements

Alberto Yúfera[1,4], Alberto Olmo[2], Paula Daza[3] and Daniel Cañete[4]
[1]*Microelectronics Institute of Seville (IMSE)*
Microelectronics National Center (CNM-CSIC),
[2]*Department of Applied Physics III,*
[3]*Department of Cell Biology,*
[4]*Department of Electronic Technology,*
[2,3,4]*University of Seville,*
Spain

1. Introduction

Many biological parameters and processes can be sensed and monitored using their impedance as marker (Grimmes, 2008), (Beach. 2005), (Yúfera, 2005), (Radke, 2004), with the advantage that it is a non-invasive, relatively cheap technique. Cell growth, cell activity, changes in cell composition, shapes or cell location are only some examples of processes which can be detected by microelectrode-cell impedance sensors (Huang, 2004) (Borkholder, 1998). The electrical impedance of a biological sample reflects actual physical properties of the tissue. In frequency dependent analyses, the β-dispersion ranging from kilohertzs to hundreds of megahertzs (Schwan, 1957) is mainly affected by the shape of the cells, the structure of the cell membranes, and the amount of intra and extra cellular solution. Electrical bio-impedance can be used to assess the properties of biological materials (Ackmann, 1993) involved in processes such as cancer development (Giaever, 1991), (Blady, 1996), (Aberg, 2004); because the cells of healthy tissues and cancer are different in shape, size and orientation, abnormal cells can be detected using their impedance as a marker.

Among Impedance Spectroscopy (IS) techniques, Electrical Cell-substrate Impedance Spectroscopy (ECIS) (Giaever, 1986), based on two-electrode setups, allows the measurement of cell-culture impedances and makes it possible to determine the biological condition (material, internal activity, motility and size) of a cell type and its relationship with the environment; for example, the transfer flow through the cell membrane (Wang, 2010). One of the main drawbacks of the ECIS technique is the need to use efficient models to decode the electrical results obtained. To efficiently manage bio-impedance data, reliable electrical models of the full system comprising electrodes, medium and cells are required. Several studies have been carried out in this field (Giaever, 1991), (Huang, 2004), (Borkholder, 1998), (Joye, 2008), (Olmo, 2010), some of them employing Finite Element simulation (FEM) for impedance model extraction. These models are the key for matching electrical simulations to real system performances and hence for correctly decoding the results obtained in experiments.

The use of FEM analysis with programs such as FEMLAB (Huang, 2004) considers that the DC mode can be employed for sinusoidal steady-state calculation by assigning complex conductivity. This works because the Poisson equation has the same form as the Laplace equation in the charge-free domain. In this chapter we will describe an alternative method of performing FEM simulations of electrode – cell interfaces based on COMSOL. The quasistatic mode of COMSOL is used, which also takes into account magnetic fields to calculate electrical impedance. The models obtained are successfully applied as loads for full electrical system modelling and simulation. In this sense, any biological sample could be electrically modelled and simulated, facilitating reliable information about integrated circuit design for impedance measuring (Yúfera, 2010b). This work includes several improvements to the model in (Huang, 2004), both to the cellular membrane and to the cell-electrode gap region. Impedance changes on small electrodes (32 μm square) caused by 3T3 mouse fibroblasts are simulated in order to validate the model and characterize the microelectrode sensor response to cell size and growth.

The knowledge acquired from the electrode-cell model can be used to create a set of applications useful in cell culture biometry and for improving efficiency biology lab tasks. One use is the detection of cell sizes by characterizing the model in terms of cell-area overlap. Impedance sensor sensitivity curves with cell size will be presented. As an extension of the application for the aforementioned sensitivity curves, a technique for measuring the cell index (CI) coefficient in cell-culture growth processes will be presented and we will show how, as a consequence of this, cell toxicity experiments can be monitored in real-time. An Analog Hardware Description Language (AHDL) model (SpectreHDL) for the mixed-mode simulation of full (electronic and biological) systems will also be described.

By applying the developed model to ECIS curves obtained experimentally, it will be possible to determine cell density and toxin-caused cell death rates. Moreover, cell modelling has recently been applied to cell imaging or bioimpedance microscopy. In (Linderholm, 2006) Electrical Impedance Tomoghaphy (EIT) techniques were reported for cell motility detection. The models proposed can also be applied to decode impedance measurements obtained from cell culture measurements, producing a two dimensional cell location map; that is, a microscopy image based on bio-impedance measurements (Yúfera, 2011).

Having explained the objectives of the work, the proposed contents of this chapter are as follows. The second section gives a brief overview of electrode solution models useful for cell-electrode characterization. The third section presents a useful method for generating cell-electrode electrical models based on COMSOL multiphysics software. The fourth section describes the finite element simulations performed. Processes for extracting useful models are included in the fifth section, which also illustrates cell size detection simulations on a simplified system. AHDL models are presented in sixth section. The seventh section covers the real time monitoring of the cell under cultivation and the application of the proposed model in dosimetric experiments. Finally, in the eighth section, a two dimensional approach to bioimpedance microscopy is described, based on the models previously developed. Conclusions are given in the ninth section.

2. The electrode – electrolyte electrical model

The impedance of electrodes in ionic liquids has been researched quite extensively (Robinson, 1968), (Schwan, 1963), (Simpson, 1963), (Schwan, 1992), (Onaral, 1982) and (Onaral, 1983). When a solid (including metals, semiconductors, and insulators) is immersed

in an ionic solution, ions in the solution can react with the electrode and the solid ions from the electrode can enter the solution, leading to complex reactions at the interface. An electrified interface or double layer develops at the interface of the two phases. Eventually, electrochemical equilibrium is established at the interface: the current flowing into the electrode is equal but opposite in sign to that flowing out from the electrode. The net result is the development of a charge distribution at the interface with an associated electric potential distribution. The Helmholtz-Gouy-Chapman-Stern model is the commonly accepted model for describing the charge distribution at the electrode interface (Bockris, 1970).

The negatively charged electrode attracts hydrated ions with positive charges to the surface but repels negatively charged ions away from the surface, yielding the profiles of cation and anion concentration C+ and C-, respectively. The water dipoles are also reoriented under the electric fields. Some ionic species that are not obstructed by their primary hydration sheath, such as some anions, can make their way to and come into contact with the electrode. Most cations have a water sheath due to their lower dissolvation energy (Bockris, 1970) and a smaller contact angle with water dipoles. The charge distribution extends to the bulk solution thanks to thermal motion, forming an ion cloud-like diffusion layer and a charge spatial distribution. The profile of the diffuse zone depends on the Debye length, which in turn depends on the gas constant, the temperature, the ion charge number and the ion concentration of the bulk solution. (Borkholder, 1998).

When a sufficiently small sinusoidal current is applied to the electrode at equilibrium, the electrode potential will be modulated by a sinusoidal overpotential (Schwan, 1968). In the range of linear behavior, the phasor ratio of the output overpotential to the input current defines the AC polarization impedance. During the small current perturbation, charge transfer due to chemical reactions and mass diffusion all occur at the electrode surface. The rate determining step will dictate the electrode polarization impedance.

In the following paragraph, we will first discuss an equivalent circuit representing all the phenomena occurring at the electrode-solution interface and then we will explain each component in the circuit. The electrified interface can be considered as the series connection of two parallel-plate capacitors with the thicknesses of a compact layer and a diffuse layer respectively and with a water dielectric. This is the electrode-solution interfacial capacitance of the electrified double layer. Apart from the double layer capacitance C_I, the electrode-solution interface has faradic impedance representing a barrier to current flow between the electrode and the solution, including the finite rate of mass transport and electron transfer at the electrode surface. These phenomena are modelled in the equivalent circuit in Fig. 1, in which the faradic impedance is in parallel with the double layer capacitance.

The current flowing through the electrified interface will encounter a resistance R_{ct} caused by the electron transfer at the electrode surface and Warburg impedance Z_W due to limited mass diffusion from the electrode surface to the solution. As a result, in the equivalent, the electron transfer resistance R_{ct} is in series with the mass diffusion limited impedance Z_W. As the current spreads to the bulk solution, the electrode has a solution conductivity-determined series resistance, represented as spreading resistance R_S in the equivalent circuit.

2.1 Double layer capacitance (C_I)

The region between the electrode surface and the Outer Helmhotz Plane (OHP) consists mostly of water molecules (Borkholder, 1998). The thickness of the OHP layer is x_H (distance from the metal electrode to OHP), and consequently the capacitance of the Helmholtz layer C_H is given by,

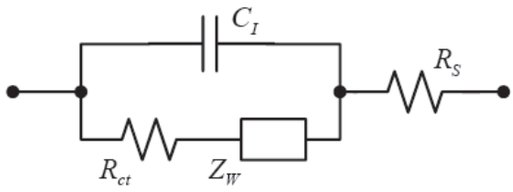

Fig. 1. Equivalent circuit for electrode solution interface. C_I is the double layer capacitance, Faradic impedance includes Z_w, the Warburg impedance and R_{ct}, the charge-transfer resistance. R_s is the spreading resistance.

$$C_H = \varepsilon\varepsilon_0 / x_H \quad (1)$$

The capacitance of the diffuse layer can be derived by differentiating the surface charge with respect to the potential. The total interfacial capacitance C_I of the electrified double layer consists of the series combination of the Helmholtz compact layer and the diffuse layer.

$$1 / C_I = 1 / C_H + 1 / C_G \quad (2)$$

where C_H is the capacitace of the Helmholtz layer described earlier and C_G is the Gouy-Chapman capacitance due to the diffuse ion cloud.This double layer capacitance has been studied in many works (Borkholder, 1998), (Schwan, 1968), (Simpson, 1980), (De Boer, 1978) although most of them agree on the value of C_I. (approximately 15μF/cm²).

2.2 Warburg impedance (Z_w)

Warburg impedance is related to the mass diffusion process occurring in the electrode-electrolyte interface (Warburg, 1899). In AC measurements, in response to the sinusoidally varying potential, the ion concentration gradient at the interface increases with frequency and the ions diffuse less as frequency increases. The Warburg impedance follows this expression,

$$Z_w = \frac{\omega^{-1/2}.K_w}{A_e.(1+j)} \quad (3)$$

where A_e is electrode area and K_w [$\Omega \cdot sec^{-1/2} \cdot cm^2$] is a constant determined by the electrochemistry and mobility of the ions involved in the charge transfer reaction. It is difficult to find a theoretical value for K_w, which in some works seems to be a parameter that is included in the model to adapt the model to experimental measurements (Huang, 2004). In other works, this impedance is not taken into account, because it is considered negligible for the materials and frequency range used in electrophysiological experiments (Joye, 2008). D. A. Borkholder, in his thesis, gives some reference values for Z_W for circular bare platinum electrodes of different sizes (Borkholder, 1998).

2.3 Charge transfer resistance (R_{ct})

Charge transfer resistance is determined by the electron transfer rate at the interface. Electrodes made of noble metal electrodes such as platinum, gold etc., in physiological saline solution act as catalytic surfaces for the oxygen redox reactions (De Rosa, 1977), (Bagotzky, 1970). The reaction rates for the anodic and cathodic processes are not the same. In the state of equilibrium, the interface current due to oxidation is equal but of the opposite

sign to that caused by reduction. Additional potential applied to the electrode will cause a net current flow. In the range comparable to the equilibrium current, the electrode behaves as a linear resistive component the resistance of which is referred to as the charge transfer resistance. As the voltage increases, the excess current increases exponentially and the charge transfer resistance decreases exponentially with the applied voltage. The charge transfer resistance can be described as,

$$R_{ct} = \frac{V_t}{J_o.z} \tag{4}$$

where J_o is the exchange current density (A/cm²), V_t is the thermal voltage (KT/q) and z is the valence of the ion involved in the charge transfer reaction.

2.4 Spreading resistance (R_s)

The final circuit element which must be included in the basic electrode/electrolyte model is the spreading resistance. As the name implies, this resistance models the effects of the spreading of current from the localized electrode to a distant counter electrode in the solution. It can be calculated by integrating the series resistance of solution shells moving outward from the electrode, where the solution resistance (R in Ω) is determined by

$$R_s = \rho L / A \tag{5}$$

where ρ is the resistivity of the electrolyte (Ω*cm), L is the length between sensing and counting electrodes (cm) and A is the cross-sectional area (cm²) of the solution through which the current passes. A similar expression is used in most models (Borkholder, 1998), (Joye, 2008).

3. Finite Element Model (FEM)

3.1 Cell electrode model

We first explored the work performed by Huang et al., making use of the computational advantages offered by COMSOL (http://www.comsol.com) over FEMLAB. Our objective was to obtain a model for the impedance changes caused by cell growth on electrodes similar in size to the cell. The cells modeled in the simulation were 3T3 mouse fibroblasts, which closely attach to surfaces and which typically have a cell-surface separation 0.15μm. The cells are about 5 μm in height and, seen from above, are irregularly shaped and approximately 30–50 μm in extent. A circular cell 30 μm in diameter centered on a 32x32 μm square sensing electrode was considered. (see Fig. 2). The sensing electrode was surrounded by a counter electrode with a considerably greater area.

3T3 mouse fibroblasts consist of a thin (about 8 nm), poorly conducting membrane surrounding a highly conductive interior (Giebel, 1999). The cell culture medium simulated by Huang et al. is highly ionic and possesses a conductivity of approximately 1.5 S/m. The cell culture medium fills the cell-electrode gap and forms an electrical double layer (Helmholtz plus diffuse layer) approximately 2 nm thick between the bulk of the medium and the electrode.

Some approximations were made by Huang et al. to address the problem using FEMLAB. Only one quarter of the electrode was simulated. As the problem involves a wide range of distance scales, it was difficult to solve by finite-element techniques, so the following adjustments were made:

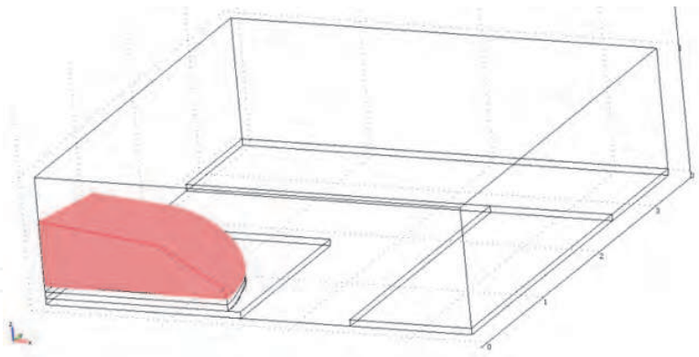

Fig. 2. Geometry of the model simulated in COMSOL.

- The electrical double layer modelling the electrode-solution equivalent circuit was replaced with a 0.5 μm thick region with the same specific contact impedance.

$$\sigma_{dl} + j2\pi f\varepsilon_{dl} = t.\left[\frac{(2\pi f)^{0.5}}{K_w} + j\frac{(2\pi f)^{0.5}}{K_w} + jC_I 2\pi f\right] \tag{6}$$

  where σ_{dl} and ε_{dl} are the conductivity and dielectric permittivity of the double layer, t is the thickness of the region, C_I is the interfacial capacitance per unit area, comprising the series combination of the Helmholtz double layer and the diffuse layer, and K_w is a constant related to the Warburg impedance contribution.
- The cell membrane was replaced by a 0.5 μm thick region with the same capacitance per unit area,

$$c_m = t.C_m \tag{7}$$

  where C_m is the membrane capacitance per unit area and t = 0.5 μm.
- The electrode-cell gap was replaced with a 0.5 μm thick region with the same sheet conductivity, that is

$$\sigma_{gap} = \frac{t_{cell-electrode}}{t}.\sigma_{medium} \tag{8}$$

  where $t_{cell\text{-}electrode}$ is the gap thickness and t is again 0.5 μm.

In our study we adopted the geometry of their simulation (see Fig. 2), and the values for the conductivity and permittivity of the electrical double layer were calculated following the same expression as shown eq. (6), with the same values for K_w and C_I as those mentioned in (Huang, 2004). Conductivity of the cell and the medium was also set to 1.5 S/m in our work. However, the model used by X. Huang et al. for the electrode-cell gap and the cellular membrane (eqs. 7 and 8) was refined as shown in the following section.

3.2 Model enhancement

Several modifications were made in the model in order to simulate cell impedance measurements more accurately and obtain a more complex model that reflected real experiments in a more realistic way. These modifications were made in the following areas.

3.2.1 Cell membrane

The equivalent circuit of the attached membrane was modeled as a resistance R_m in parallel with a capacitance C_m, in a similar way to that reported in (Borkholder, 1998). These parameters are defined as,

$$R_m = \frac{1}{g_m.A_e} \qquad C_m = c_m.A_e \tag{9}$$

where A_e is the area of the attached membrane (in our case A=706.86x10^{-12} m^2), g_{mem} = 0.3 mS/cm^2 is the local membrane conductivity and c_{mem} (1 μF/cm^2) is the membrane capacity per unit area. We can calculate the conductivity and permittivity of the cellular membrane from the impedance using the following expression

$$Z = \frac{1}{K.(\sigma + j\omega\varepsilon)} \tag{10}$$

where K is the geometrical factor (K = area / length). In our case a value of 5 μm was taken as the length. (This value corresponds to the thickness of the membrane layer represented in COMSOL). The value obtained for K was 1.413.10^{-3}, and the values obtained for conductivity and permittivity were σ =1.5 μS/m and ε = 5.001 nF/m (ε_r=565).

3.2.2 Cell membrane-electrolyte interface capacitance

This capacitance was not considered in Huang´s model, but may also be important, as it models the charge region (also called the electrical double layer) which is created in the electrolyte at the interface with the cell. The capacitance C_{hd} is defined as the series of three capacitances,

$$C_{h1} = \frac{\varepsilon_0\varepsilon_{IHP}}{d_{IHP}}.A_{ce}$$
$$C_{h2} = \frac{\varepsilon_0\varepsilon_{OHP}}{d_{OHP} - d_{IHP}}.A_{ce} \tag{11}$$
$$C_d = \frac{q\sqrt{2\varepsilon_0\varepsilon_d KTz^2 n^0 N}}{KT}.A_{ce}$$

where A_{ce} is the area of the attached membrane, ε_0 is the dielectric permittivity of free space; ε_{IHP} and ε_{OHP} are, respectively, the Inner and Outer Helmholtz Plane relative dielectric constant; d_{IHP} is the distance from the Inner Helmholtz Plane to the membrane; d_{OHP} is the distance from the Outer Helmholtz Plane to the membrane; ε_d is the diffuse layer relative dielectric constant; K_B is Boltzmann's constant; T is the absolute temperature; q is the electron charge; z is the valence of ions in the solution; n_0 is the bulk concentration of ions in the solution; and N is the Avogadro constant.

For C_{hd}, the values given in (Joye, 2008) are considered. In particular, it is assumed that ε_{IHP} = 6, ε_{OHP} =32, d_{IHP} = 0.3 nm, d_{OHP} = 0.7 nm, z = 1, T = 300 K, and n_0 =150 mM. The area of the attached membrane is in our case A_{ce}=706.86 μm^2 and ε_d is set to 1. The following values were obtained: C_{h1}= 0.125pF; C_{h2}=0.5pF; C_d=2.22pF, and the total series capacitance was

C_{hd}=0.1pF. Comparing the impedance equivalent to this capacitance with the same expression as before (eq. 10), and remodelling this layer as a 5 μm thick layer with K =1413.10^{-6}, we obtained ε=0.0011 uF/m, which corresponds to ε_r = 124.29, the value that was loaded into COMSOL.

4. COMSOL Simulations

As can be seen in Fig. 2, only one quarter of the electrodes and the cell was simulated. Electrodes were modeled with no thickness. The first layer modeled on top of the electrode surface was the 0.5 μm thick electrical double layer, which can be seen in the figure. On top of the electrical double layer, the cell-electrode gap was modeled with another 0.5 μm layer. In our simulation this layer included the cell membrane-electrolyte interface capacitance. Finally, on top, we have the cell membrane, also modeled as another 0.5 μm layer, and the rest of the cell. For each layer, it is necessary to load the conductivity and permittivity values calculated earlier into COMSOL. All surfaces had an insulating boundary condition (n*J=0) with the exception of the surfaces separating the different layers and sub-domains within the model, which were set to continuity (n.(J_1-J_2) = 0), and the bottom surfaces of the two electrodes, which were set to an electric potential of 1V and 0V.
The Quasi-statics module of COMSOL was used to perform the finite element simulations. In this mode, it is possible to obtain the solution for the electric potential for different frequencies. The simulations were performed on a 2.26 GHz Intel(R) Core(TM)2 DUO CPU. Solution times varied with the frequency but ranged from 3 to 6 minutes. In Fig. 3 we can see the solution for the electric potential at the determined frequency of 100 Hz.

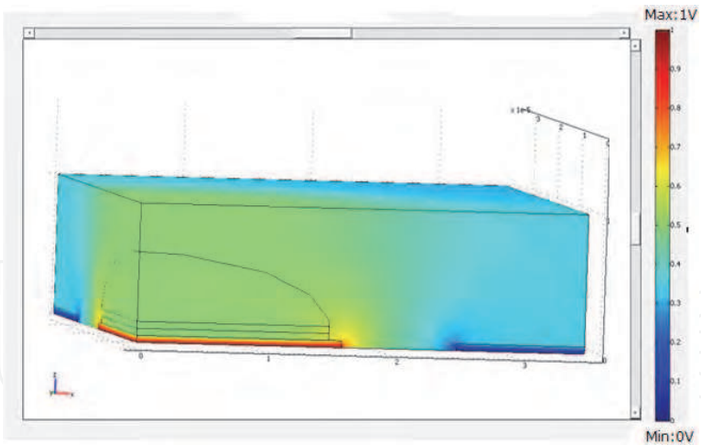

Fig. 3. Electric potential solution at 100Hz.

Two series of simulations, at frequencies ranging from 10^2 Hz to 10^6 Hz, were made with and without the presence of the cell. Once the solution for the electric potential had been found by COMSOL, Boundary Integration was used to find the electric current through the counter electrode. With that value the electric impedance was calculated, taking into account that the voltage difference between electrodes was 1V and that impedance had to by divided by 4 (as only one quarter of the electrodes was being simulated.) The values obtained are shown in Fig. 4.

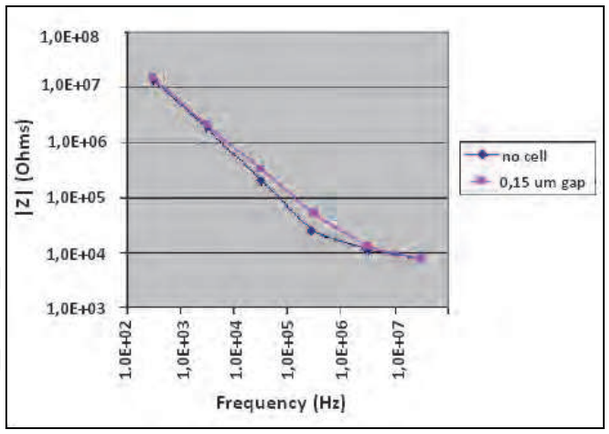

Fig. 4. Impedance magnitude of the microelectrode system with (red line) and without (blue line) the cell.

The measured impedance changes by several orders of magnitude over the simuated frequency range, in accordance with previous works (Schwan 1992), (Onaral, 1982). It can be appreciated how the presence of the cell changes the measured impedance, with the biggest change recorded at a frequency near to 10^5 Hz. This also corroborates the study carried out by (Huang, 2004). Another way of representing the impedance magnitude is to observe the impedance changes in the system with the cell on top with respect to the microelectrode system without cell. This can be done by plotting the normalized impedance change with respect to the cell-less system, defined as

$$r = \frac{Z_c - Z_{nc}}{Z_{nc}} \tag{12}$$

where Z_c and Z_{nc} are the impedance magnitudes with and without cell, respectively. The normalized impedance changes in the system with the 30 μm-diameter cell modelled earlier is plotted in Fig. 4 (red line). Figure 5 shows the normalized impedance parameter, r, as a function of frequency. It can be seen how the 100 kHz frequency seems to be the optimal value for sensing the cell, since sensor sensitivity is maximum.

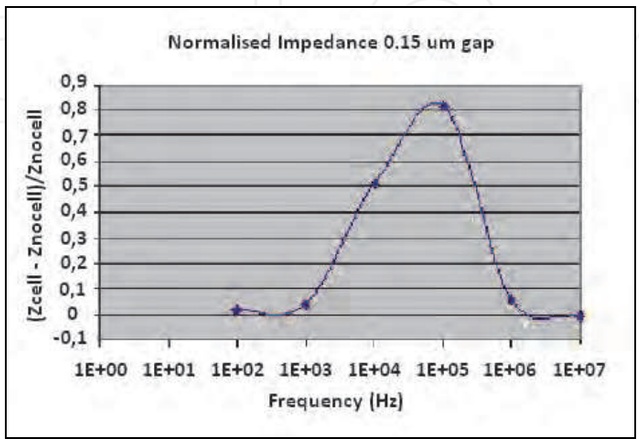

Fig. 5. Simulated normalised impedances of the system, for a 30 μm cell diameter.

5. Model extraction process

Figure 6 shows an example of a two-electrode impedance sensor useful for the ECIS technique: e_1 is called the sensing electrode and e_2 the reference electrode. Electrodes can be manufactured in CMOS process with metal layers (Huang, 2004) or using post-processing steps (Manickam, 2010). The cell location on top of e_1 must be detected. Circuit models developed to describe electrode-cell interfaces (Huang 2004, Joye 2008) contain technology process information and take the cell-electrode overlap area as their main parameter. The correct interpretation of these models gives information for: a) *electrical simulation*: parametrized models can be used to update the electrode circuit in terms of its overlap with cells, b) *imaging reconstruction*: electrical signals measured with sensors can be associated with a given overlap area, making it possible to obtain the actual covering on the electrode from experimental results.

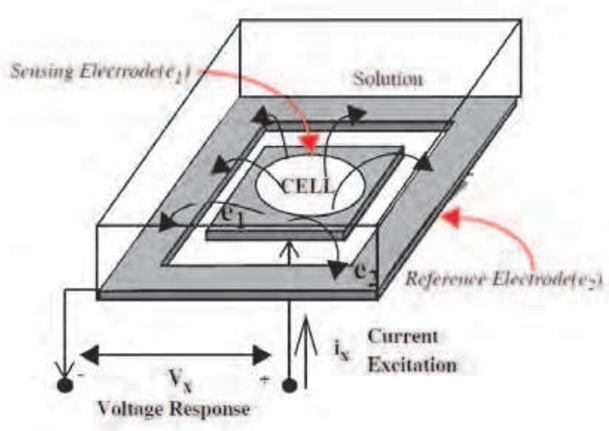

Fig. 6. Basic concept for measuring with the ECIS technique using two electrodes: e_1 (sensing electrode) and e_2 (reference electrode). AC current i_x is applied between e_1 and e_2, and voltage response V_x is measured from e_1 to e_2, including the effect of e_1, e_2 and sample impedances.

This work employs the electrode-cell model reported in (Huang 2004, Olmo 2010), obtained using finite element method simulations. The model in Fig. 7 considers that the sensing surface of e_1 could be total or partially filled by cells. For the two-electrode sensor in Fig. 6, with e_1 sensing area A, $Z(\omega)$ is the impedance by unit area of the empty electrode (without cells on top). When e_1 is partially covered by cells in a surface A_c, $Z(\omega)/(A-A_c)$ is the electrode impedance associated with the area not covered by cells, and $Z(\omega)/A_c$ is the impedance of the area covered. R_{gap} models the current flowing laterally in the electrode-cell interface, which depends on the electrode-cell distance at the interface (in the range of 15-150 nm). R_s is the spreading resistance through the conductive solution. For an empty electrode, the impedance model $Z(\omega)$ is represented by the circuit in Fig. 1. For e_2, not covered by cells, the model in Fig 7a was considered. The e_2 electrode is typically large and grounded, and its resistance is small enough to be rejected. Figure 8 represents the impedance magnitude, Z_c, for the sensor system in Fig. 6, considering that e_1 could be either empty, partially or totally covered by cells. The parameter *ff*, called the *fill factor*, can be zero for $A_c = 0$ (e_1 electrode empty), and 1 for $A_c = A$ (e_1 electrode full). Z_c (*ff*=0)= Z_{nc} is defined as the impedance magnitude of the sensor without cells.

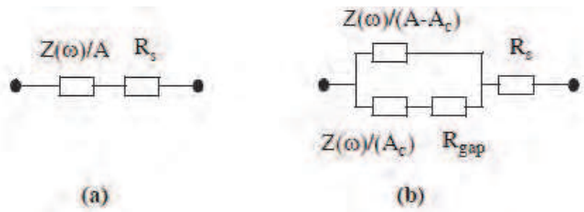

Fig. 7. Proposed model for an electrode-solution-cell model with area A, uncovered by cells (a) and covered over area A_c (b).

The relative changes in impedance magnitude, defined in eq. (12), inform more accurately from these variations: r is the change in impedance magnitude for the two-electrode system with cells (Z_c) as compared to the system without cells (Z_{nc}). Figure 9 shows the *r* versus frequency graph plotted for cell-to-electrode coverage ff from 0.1 to 0.9 in steps of 0.1, using a R_{gap} = 90 kΩ. The size of the electrode is 32 x 32 μm². Again we can identify the frequency range where the sensitivity to cells is high [10 kHz, 1 MHz], represented by r increments. For a given frequency, each value of the normalized impedance r can be linked with its ff, allowing cell detection and estimation of the covered area A_c. Electrodes can be manufactured (in terms of technology and size) according to r-sensitivity curves to improve sensor response.

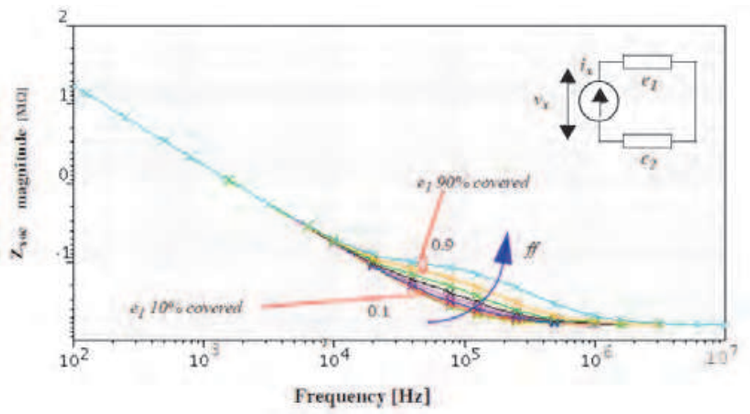

Fig. 8. Impedance evolution when fill factor increases 32 x 32 μm² for a 32 x 32 μm² electrode.

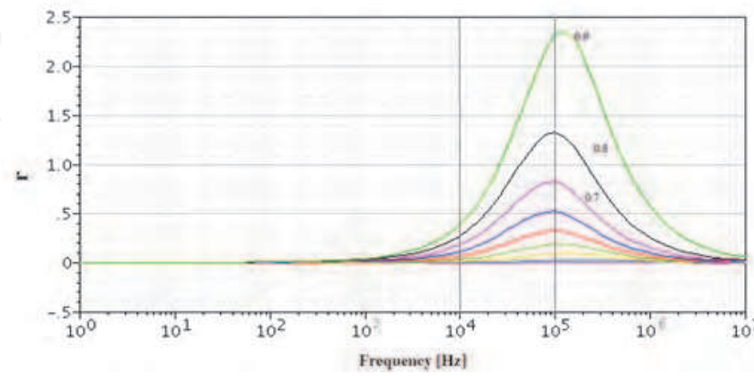

Fig. 9. Normalized impedance r parameter evolution versus frequency. Each line corresponds to values of the fill factor (or A_c covered by cells) in the range of 0.1 (nearly empty) to 0.9 (nearly full).

From Fig. 9, it can be deduced that electrode-cell electrical performance models can be used to derive the overlapping area in a cell-electrode system, an useful resource for biological studies. It can be observed how the curve matches with the frequency range, placing the maximum r value at around 100 kHz, as predicted in the COMSOL simulations. A value of R_{gap} = 90 kΩ was selected for this curve, representing a maximum value of the r curve with ff = 0.69, which in turn represents the ratio (A_c/A), for the cell size of 30 μm diameter shown in the figure obtained using FEM simulations. Other cell sizes, with different diameters, can be selected from the r curves in Fig. 9.

6. AHDL model for simulation

Electrical simulations are commonly employed by electrical engineering designers to obtain useful information and predictions about circuit performance before circuits are sent to the factory. Simulations of front-end sensor data acquisition circuits must be trained versus real sensor models, so a reliable representation of a sensor is a prerequisite for a correct acquisition circuit design. The modelling process for an impedance sensor, as described in this work, can be performed using Analog Hardware Description Language (AHDL), which can easily be incorporated into mixed-mode simulators as SpectreHDL. Another advantage of using AHDL modelling is the possibility of incorporating non-linear circuit element performance, in our case the frequency square root function in the Warburg impedance. This makes AHDL models widely applicable, allowing accurate electrode-solution model simulation, and enabling their incorporation into mixed-mode simulators.

6.1 AHDL model

The proposed model has three main parameters: the electrode area (A), the fill-factor (ff) or percentage of the electrode area covered by cells, and the resistance of the gap region (R_{gap}). Technological data is also included, defining the physical properties of the sensor material and the solution. The HDL model directly implements the equations for circuit elements described in section 2: capacitor double layer, transfer resistance, Warburg resistance and spreading resistance, considering technology information (Borkholder, 1998) and parameters A, ff and R_{gap}. An example with the R_{ct} resistance is described in the following lines:

```
// Resistor transfer: Rct
// Spectre AHDL for AHDL_ELEC, resistor_transfer, ahdl
module resistor_transfer(pin,nin) (A,FF,T)
node [V,I] pin, nin;
parameter real A = 2500p;
parameter real FF = 0.0;
parameter real T = 309;
{
real curr_density = 2.0e-5;                 /* Amp/m2 Au-sol reaction*/
real z_ions = 1.0;                          /* Valence ions */
real q_e =1.6e-19;                          /* Charge e- */
real K   =1.3806e-23;                       /* Constant Boltz. J/°K */
real v_thermal = 0.0;                       /* Thermal V. */
real rt = 0.0 ;                             /* ohm.m2 */
analog {
       v_thermal = K*T/q_e;
       rt = (v_thermal/(curr_density*z_ions));
       rt = rt / A*(1.0-FF);
```

```
        I(pin,nin) <- (V(pin,nin)/rt);
        }
}
```

Analog Hardware Description Language (AHDL) offers an easy way to describe equivalent circuits for the electrode-solution-cell model in Figure 1. Each circuit element is connected using its node description. Inside, the corresponding equations are incorporated to describe its electrical performance, technology data, geometry parameters (A) and model values (R_{gap}). This cell-electrode description can be used to carry out electrical simulations.

6.2 SpectreHDL simulations

In this section we present some simulation results obtained when modelling a commercial electrode: ECIS 8W10E, from Applied Biophysics Inc. (http://www.biophysics.com). A photograph of the complete system is shown in Fig. 10. Eigth wells can be seen, each one containing ten circular gold microelectrodes, of 250 μm diameter. This impedance sensor will be employed for the cell culture experiments described in section 7. For electrical simulations, ten identical electrodes will be considered in parallel. The HDL model for each one is described using the circuit equations from section 2 and the model in Fig. 7b.

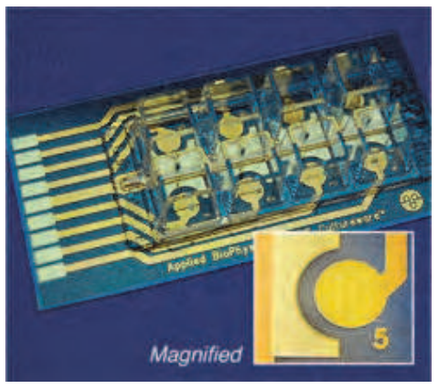

Fig. 10. Electrode employed for impedance measurements.

The expected performance of ten circular electrodes is illustrated in the following simulations. Ten sensing electrodes were used (e_1 in Fig. 6), with just one common reference electrode (e_2), much larger than the sensing electrodes. Also shown are the electrode area dependence (A), the fill factor dependence (ff), and the resistance gap dependence (R_{gap}), to illustrate the model's flexibility in different environments. Fig. 11 represents the normalized impedance r-values expected for these electrodes, for R_{gap} = 22 kΩ, when the fill factor changes from a situation of electrodes uncovered by a cell (ff = 0.1) to nearly fully covered (ff = 0.9). Different cell densities or sizes can be detected using these sensitivity curves. Several values of R_{gap} can also be used to match the models to observed performance. In Fig. 12, several R_{gap} values were set for ff = 0.9, resulting in large changes in r-values. These parameters are used to apply the proposed model to a specific cell line or cell culture experiment. Finally, the electrode area for R_{gap} = 22 kΩ and ff = 0.9 was also changed. In this way, electrode frequency response can be set for the experiment's given electrode geometry and technology parameters (Fig. 13). From these simulated results, it can be observed that optimal working frequency is close to the frequency proposed by the electrode factory (around 4 kHz), and that the electrode area covered by cells can be simulated using the fill factor parameters, making it possible to study cell density and size from the proposed model and simulations.

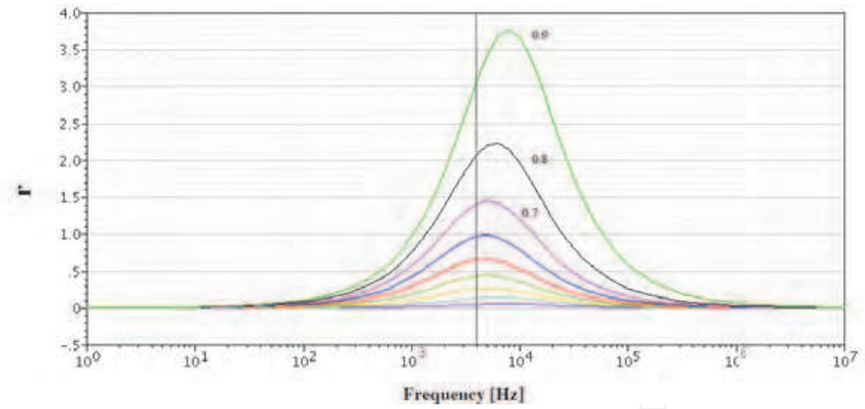

Fig. 11. The r versus frequency curves obtained for ff ∈ [0.1,0.9] and R_{gap} = 22 kΩ, using the data from 8W10E electrodes.

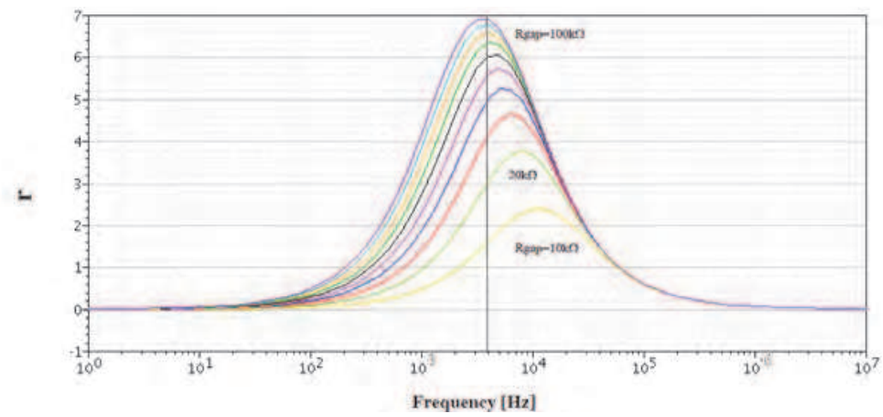

Fig. 12. The r versus frequency curves obtained for R_{gap} ∈ [10 kΩ,100 kΩ] in steps of 10kΩ, for ff = 0.9, using the data from electrodes 8W10E.

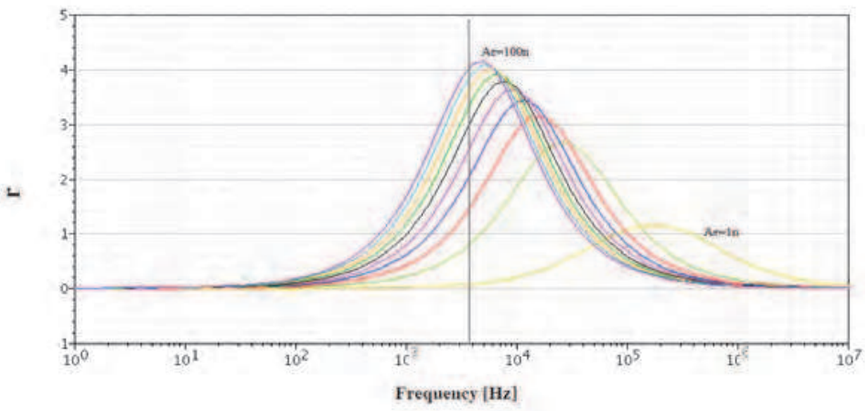

Fig. 13. The r versus frequency curves obtained for R_{gap} = 22 kΩ and ff = 0.9, for different values of the electrode area: 49n (49.10^{-9} m²) corresponds to a circular electrode with a 250 μm diameter.

6.3 Model extraction

The performance curves obtained above can be used to match experimental results to model parameters and obtain relevant biometric characteristics like cell size, cell culture density and gap resistance. Specific cell parameters such as size and cell density can be obtained from the fill factor values. Gap resistance value provides information about the cell type, because it is related to cell adhesion and cell membrane electrical performance. Models can thus be predicted from FEM simulations performed using the modelling procedure mentioned in section 2. This means that the experimental performance observed in labs can be matched to fit proposed model for the real time monitoring and interpretation of biological experiments, especially cell culture protocols.

7. Cell culture applications

In this section, we present some applications for the cell-electrode electrical model developed earlier. The objective is to employ the information obtained from model electrical simulations to interpret cell culture experiments and to provide information about cell size, cell culture growth processes and cell dosimetric characterization.

7.1 Size definition

Cell size can be measured directly from the fill-factor parameter using the sensor curve sensitivities in Figures 11 to 13. There, maximum sensitivities to cell size (maximum *r* values) are obtained at several frequency ranges (10 kHz to 1 MHz in Fig. 9). Cell size testing should be performed after detection of the optimum frequency range. Another consideration is that the electrode size should be of the same order as the cell size to be detected using the maximum sensitivity delivered by the impedance sensor. This figure demonstrates that cells of different sizes can be detected at a given working frequency by measuring their corresponding normalized impedance value.

7.2 Cell growth

In normal conditions, a cell generates one replica (divides in two equal cells) in a cell cycle, specific to each cell line, which may take several hours. Impedance sensors can be used to measure the number of cells in a cell culture experiment, because the cells are attached to the bottom electrode when they are not dividing. As the number of cells increases, the total bottom area covered by cells increases too, increasing the number of cells placed on top of an electrode and so in time, raising the impedance measured from the electrodes. In normal protocols, growth rate is measured by a tedious process that requires seeding a number of dishes equal to the number of time points to be represented, and counting the number of cells in each dish everyday. Fig. 14a shows a growth curve we measured over seven days using 8W10E sensors in a similar setup to that described in (Giaever, 1986). An initial number of approximately 5000 AA8 cells from chinese hamsters was seeded. From this curve, impedance dynamic range is around 1220 Ω, from 380Ω to 1600 Ω. Considering the initial cell number of 5000 cells very low, we can take the initial impedance as due to the no-cell impedance value (Z_{nc}). At t = 6000 min, the medium was changed, and the confluent phase was achieved at t = 8500 min, approximately. The maximum experimental value given in eq. (12) is around r = 3.1, as illustrated in Fig. 14b. If we consider that in our model the electrodes are almost fully covered by cells (ff = 0.9), the best matching value of R_{gap} is 22 kΩ. System response corresponds to the r-values illustrated in figures 11 and 12. From these curves, the fill factors at different times can be obtained. Table I summarizes the

relative normalized impedance values r at several times. Using Fig. 15 to represent the sensor response, it is possible to obtain the corresponding fill factor at every instant. The number of cells in real time can be estimated by considering that the number on top of each electrode can be measured in the order of 500 to 1000 cells. For a well area of 0.8 cm², the maximum number of cells goes from 0.8 10^6 to 1.6 10^6. The number of cells, n_{cell} in Table I, is obtained from 0.8x10^6, the expected final cell value. Initially, 5000 cells from the AA8 cell line were seeded. It was considered that a maximum 90% (ff=0.9) of the well surface was covered by the cells. A value of Z_{nc} = 380 Ω for r calculus at eq. (12) was also considered.

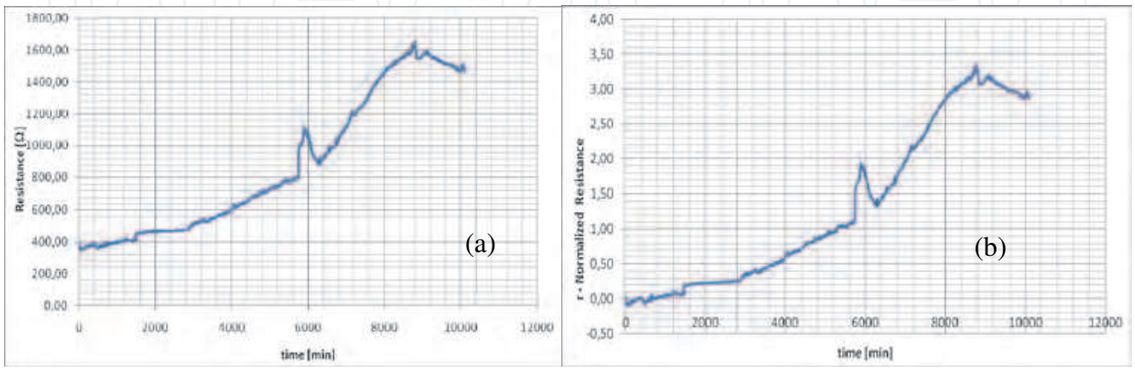

Fig. 14. (a) Impedance evolution in the cell growth experiment. (b) Estimated normalised impedance r evolution.

Table I: Number of cells (ncell) obtained from the impedance Zc measure in Fig. 14a, and using sensor curves proposed for 8W10E electrodes.

time	r	ff	n_{cell}
0	0	-	5000
500	0.024	0.020	18000
1000	0.050	0.050	44000
1500	0.072	0.070	63000
2000	n. a.	n.a.	n.a.
2500	n.a.	n.a.	n.a.
3000	0.374	0.362	322000
3500	0.437	0.395	351000
4000	0.615	0.475	422000
4500	0.777	0.530	471000
5000	0.903	581	516000
5500	1.033	0.602	535000
6000	1.074	0.620	551000
6500	1.507	0.710	631000
7000	1.970	0.775	689000
7500	2.353 --->	0.810	720000
8000	2.837	0.860	764000
8500	3.113	0.890	791000
9000	3.134	0.900	800000
9500	3.010	0.875	778000
10000	2.857	0.864	768000

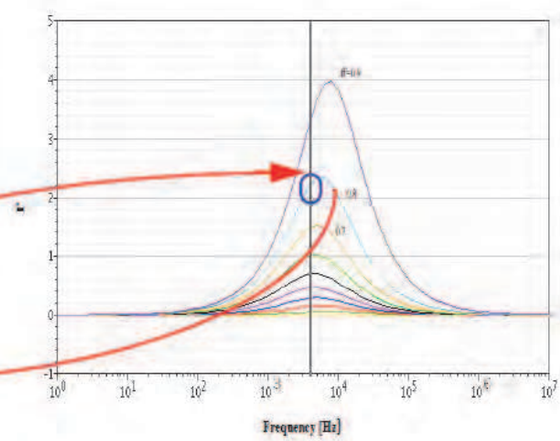

Fig. 15. Table I shows the normalized impedance r-values obtained experimentally from sensor curves in Fig. 14. ff values in Table I are obtained from experimental r-values, using curves in this figure. For example, at t = 7500 min, the measured r value is 2.353, which corresponds to ff = 0.810 on the impedance sensor curves, at the frequency of 4 kHz, and using R_{gap} = 22 kΩ.

The approximate cell number can be deduced from the last column, allowing a real time cell count based on the r-curves associated with the sensors. If different types of cells are considered, for each one the R_{gap} parameter can be calculated, producing r-curves specific to each cell line. This process allows cell lines to be identified and differentiated, for example to match the impedance measure of normal cells and cancer cells (Aberg, 2004).

7.3 Dosimetry analysis

Experiments to characterize the influence of certain drugs on cell growth were also developed. These are usually known as dosimetry protocols, and consist on determining the response of the cell growth to several drug doses. The objective is to demonstrate that the proposed model for a cell-electrode system allows cells to be selected and counted under different conditions. In our case, we again considered the AA8 cell line and, as drugs, we used six different doses of MG132 for growth inhibition, from 0.2 μM to 50 μM. After 72 hours of normal cell growth, the medium was changed and different doses of the drug were: 0.2, 0.5, 1, 5, 10 and 50 μM for wells 3 to 8 respectively. Well 2 was the control.

The experimental impedances obtained for the 8 wells are shown in Fig. 17, for a working frequency of 4 kHz. At the end of the experiment it could be observed that impedance decreases as drug dosage increases. The control well (W2) was full of cells with the maximum impedance, while the well with the maximum dosage (W8) had the lowest resistance, at the bottom. The black line (W1) represents electrode-solution impedance. In this case, after the medium change (t = 4000 min), impedance was seen inexplicably to drop below the initial baseline level (400 Ω). As in cell cultivation experiments, a resistance value was taken based on a starting value of Z_{nc}, as a value representative of electrode-solution impedance. Final impedance values at 8000 min, Z_{c},, were considered as the final response, in Table II. Considering Z_{nc} and Z_{c}, r values are calculated in the third column. The r versus frequency curves in Fig. 15, can be used to obtain the estimated ff values from the proposed model. The number of cells at the end of the experiment was also counted, and is shown in the last column for each well. Considering ff_{max} = 0.9 for an experimentally measured cell number of $8.06x10^5$, it is possible to calculate the rest of the expected ff values.

The same data is summarized in Table III for 2, 4 and 10 kHz respectively. The best match is obtained at 4 kHz in fill factor (ff parameter). The impedance baseline, Z_{nc}, for r calculus can be seen to decrease with frequency, due probably to electrode impedance dependence. For medium resistance (W1) and high drug concentration wells (W7,W8), the resistance measured is below Z_{nc}, so eq. (12) cannot be applied for r calculation.

8. Cell imaging impedance-based

Another application of the proposed model for testing cell culture impedance sensing is the implementation of an impedance based imaging system (Yúfera, 2011)(Yúfera, 2010a). This can be done when, as was commented before, cell sizes are of the same order as microelectrode sensors. In this example, we have only considered a simplified model for electrode-solution-cell electrical performance.

8.1 Cell location applications

The cell-electrode model: Fig. 19 shows the model employed for a two-electrode sensor as shown in Fig. 6. For the empty electrode, the impedance model Z(ω) has been chosen. The

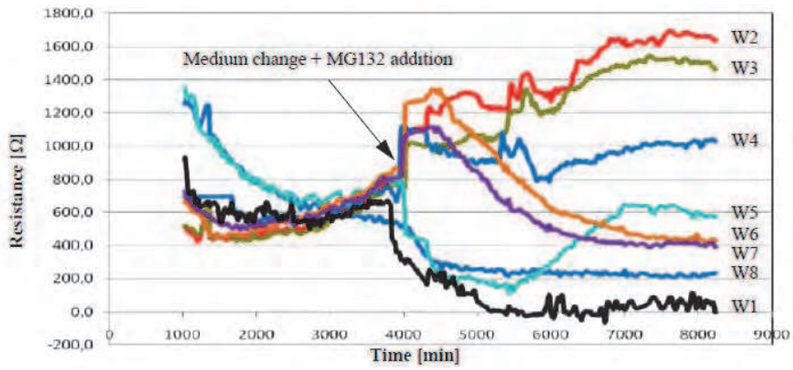

Fig. 16. Impedance obtained in 8 wells (W1 to W8) at 2 kHz frequency. W1: Medium. W2: Control. W3: 0.2µM. W4: 0.5 µM. W5: 1 µM. W6: 5 µM. W7: 10 µM. W8: 50 µM.

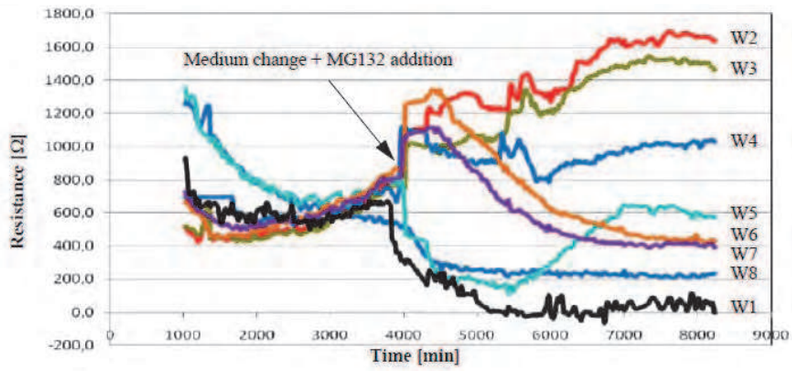

Fig. 17. Impedance obtained in 8 wells at 4 kHz frequency. (a) W1: Medium (b) W2: Control (c) W3: 0.2µM (d) W4: 0.5 µM (e) W5: 1 µM (f) W6: 5 µM (g) W7: 10 µM and (h) W8: 50 µM.

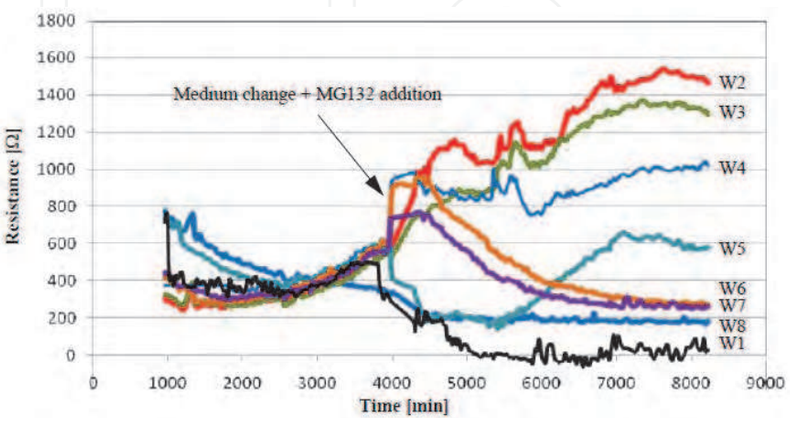

Fig. 18. Impedance obtained in 8 wells at 10 kHz frequency. (a) W1: Medium (b) W2: Control (c) W3: 0.2µM (d) W4: 0.5 µM (e) W5: 1 µM (f) W6: 5 µM (g) W7: 10 µM and (h) W8: 50 µM.

Well	Z_c at t= 8000 min	r from Z_c and $\mathbf{Z_{nc}}$	ff estimated from model	ff expected	N° cells measured
1	259.2	-	-	-	Medium
2	1631.7	3.1	0.90	0.900	$8.06x10^5$
3	1454.7	2.6	0.85	0.690	$6.13x10^5$
4	1030.6	1.5	0.72	0.610	$5.41x10^5$
5	625.8	0.5	0.44	0.410	$3.60x10^5$
6	417.4	0.05	0.037	0.036	$3.20x10^4$
7	406.8	0.015	0.016	0.024	$2.10x10^4$
8	99.6	< 0	-	0.005	$4.00x10^3$

Table II. Experimental values for relative impedance (r) and fill-factor (ff). Z_{nc} = 400 Ω. Frequency = 4 kHz.

	Z_c [Ω] at t= 8000 min			r from Z_c and Z_{nc}			ff Estimated from model			
Well	2kHz	4kHz	10kHz	2kHz	4kHz	10kHz	2kHz	4kHz	10kHz	ff expected
1	212	259.2	178	-	-	-	-	-	-	Medium
2	1650	1631.7	1500	2.43	3.1	3.76	0.98	0.90	0.90	0.900
3	1524	1454.7	1336	2.18	2.6	3.24	0.94	0.85	0.88	0.690
4	1042	1030.6	1012	1.17	1.5	2.21	0.82	0.72	0.82	0.610
5	580	625.8	580	0.21	0.5	0.84	0.32	0.44	0.44	0.410
6	432	417.4	282	-	0.05	-	-	0.037	-	0.036
7	419	406.8	267	-	0.015	-	-	0.016	-	0.024
8	84	99.6	43	-	-	-	-	-	-	0.005

Table III. Experimental values for relative impedance (r) and fill-factor (ff) at different frequencies. Z_{nc} = 480Ω, 400Ω, and 315Ω for 2, 4 and 10 kHz working frequency respectively.

circuit is shown in Fig. 19c, where C_p, R_p and R_s are dependent on both electrode and solution materials. For e_2 the model in Fig 19a, uncovered by cells, was considered. Usually, the reference electrode is common for all sensors, because its area is much higher than e_1. Figure 19d shows the relative impedance magnitude, r, for the sensor system, using a cell-to-electrode coverage ff from 0.1 to 0.9 in steps of 0.1. Again, the frequency range where the sensitivity to cells is high, represented by *r* increments, can be readily identified. For imaging reconstruction, the study in (Yúfera, 2011) proposes a new CMOS system to measure the r parameter for a given frequency, and to detect the corresponding covering area on each electrode according to the sensitivity shown in Fig 19d.

8.2 2D image applications

The case simulated was that of an 8x8 two-electrode array. The sample input to be analysed was a low density MCF-7 epithelial breast cancer cell culture, as shown in Fig. 20a. In this image some areas are covered by cells and others are empty. Our objective was to use the area parametrized electrode-cell model and the proposed circuits to detect their location. The selected pixel size was 50 μm x 50 μm, similar to cell dimensions. Figure 20a shows the grid selected and its overlap with the image. We associated a squared impedance sensor,

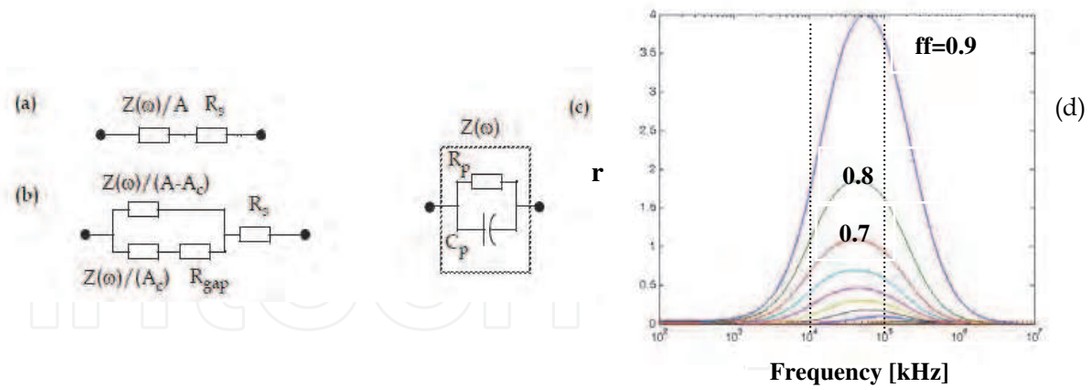

Fig. 19. Electrical models for (a) e_1 electrode without cells and, (b) e_1 cell-electrode. (c) Model for Z(ω). (d) Normalized magnitude impedance *r* for *ff*= 0.1 to 0.9 in steps of 0.1. C_p=1nF, R_p=1MΩ, R_s=1kΩ and R_{gap}=100 kΩ.

similar to the one described in Fig. 6, with each pixel in Fig. 20a to obtain a 2D system description valid for electrical simulations. An optimum pixel size can be obtained using design curves for normalized impedance *r* and its frequency dependence. Each electrical circuit associated to each e_1 electrode in the array was initialized with its corresponding fill factor (*ff*) producing the matrix in Fig 20b. Each electrode or pixel was associated with a number in the range [0,1] (ff) depending on its overlap with cells on top. These numbers were calculated to an accuracy of 0.05 from the image in Fig.20(a). The *ff* matrix represents the input of the system to be simulated. Electrical simulations of the full system were performed at 10 kHz to obtain the impedance corresponding to each electrode using the AHDL model proposed in section 6. Pixels were simulated by rows, from the bottom left hand corner (pixel 1) to the top right hand corner (pixel 64) (Yúfera, 2011).
To have a 2D graph image of the fill factor (the area covered by cells) in all pixels, values or r were obtained from the measurements taken and the sensor curves are used in Fig. 19. The results are shown in Fig 21, which represents the 8x8 ff-maps. In the maps, each pixel has a

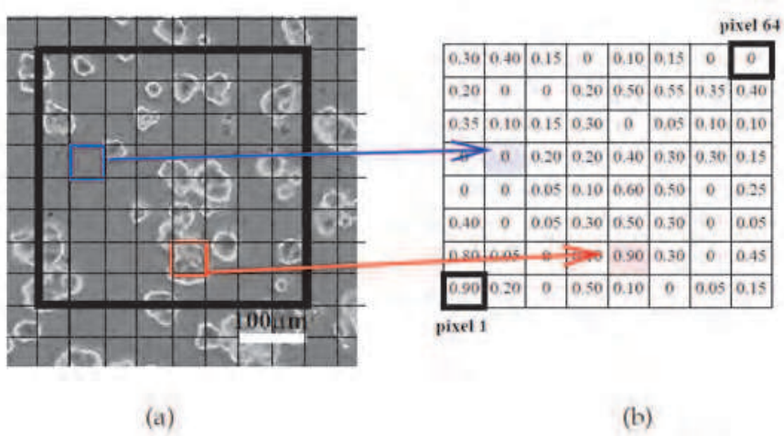

Fig. 20. (a) 8x8 pixel area selection in epithelial breast cancer cell culture. (b) Fill factor map (*ff*) associated with each electrode (pixel).

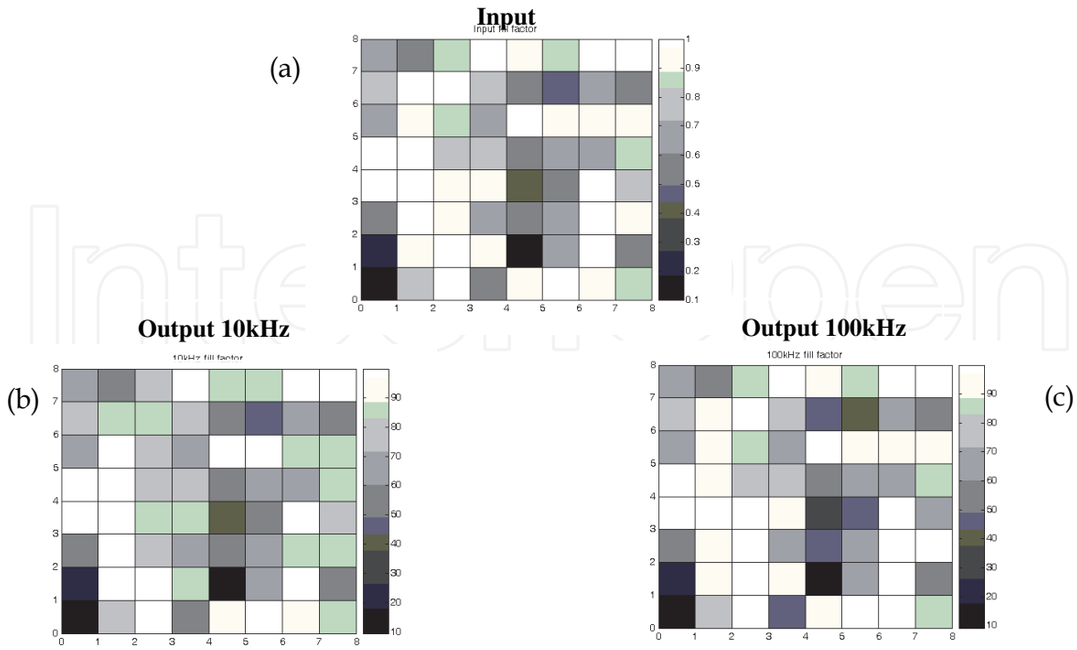

Fig. 21. 2D diagram of the fill factor maps for 8x8 pixels: (a) ideal input. Image reconstructed from simulations at (b) 10 kHz and (c) 100 kHz.

grey level depending on its fill factor value (white is empty and black full). Specifically, Fig. 21(a) shows the ff-map for the input image in Fig. 20b. Considering the parametrized curves in Fig. 19 at 10 kHz frequency, the fill factor parameter was calculated for each electrode and the results are shown in Fig. 21b. The same simulations were performed at 100 kHz, producing the *ff*-map in Fig. 21c. As Fig. 19 predicts, the best match with the input is found at 100 kHz, since normalized impedance is more sensitive and the sensor has a higher dynamic range at 100 kHz than at 10 kHz. For reported simulations, 160 ms and 16 ms per frame are required working at 10 kHz and 100 kHz, respectively. This frame acquisition time is enough for real time monitoring of cell culture systems.

9. Conclusions and discussion

The main objective of the work described in this chapter is to develop alternative methods for measuring and identifying cells involved in a variety of experiments, including cell cultures. To this end, we have focussed on obtaining models of the sensor system employed for data acquisition, and on using them to extract relevant information such as cell size, density, growth rate, dosimetry, etc.

First of all, the impedance parameter was selected as an excellent indicator of many biological processes, and Electical Cell-substrate Impedance Spectroscopy (ECIS), a technique currently considered very promising, was employed. Microelectrode impedance based sensors were analyzed, and finite element simulations carried out to model the electrical performance of both electrode-solution and electrode-solution-cell systems. This modelling process, starting with basic descriptions such as cell size, impedance, etc., enabled the use of different cells.

A practical circuit for electrode-solution and electrode-solution-cell simulation was employed, with the capacity to incorporate modelling information derived from FEM simulations. An Analog Hardware Description Model was proposed to incorporate this model to mixed-mode simulations at SpectreHDL, allowing non-linear performance characterization for the model proposed and the use of mixed-mode simulators.
Commercial 8W10E electrodes supplied by Applied Biophysics (AB) were modelled using the proposed five element circuit, obtaining good matches. Optimal measurement frequency was identified near 4 kHz, which is the frequency usually recommended by AB. Relative impedance changes were also related to the cell density thanks to fill factor parameters.
A set of experiments were conducted to match the proposed models with the performance observed at cell cultures. The first proposal was to study cell growth evolution based on 8W10E electrodes. Curves obtained experimentally, using a basic set-up, allowed real time growth to be monitored. An estimation of the number of cells was obtained using sensor curves calculated from the proposed electrical model.
Dosimetry experiments reproduce conditions similar to those of cell growth, but in this case, a growth inhibitor was added at different doses. In the experimental data, it was observed that the higher the dose, the more the measure impedance decreased, in according with the expected performance. We still do not fully understand the experimental results obtained from the measurements. Impedance inexplicably fell below the expected baseline (Z_{nc}). However, impedance curves for the control and for small drug doses were perfectly aligned up to this impedance level. A proposed model was set up with R_{gap} = 22 kΩ to explain the experimental data. Deviations from the data expected were in the order of 10% and 20% in fill factor calulations (ff), and were more precise at 4 kHz.
A final application was illustrated in the field of microscopy for cell cultures through the correct decoding of impedance response. By calculating the fill factor, it is possible to define the area occupied over one microelectrode.
As mentioned earlier, deviation in the fill factor determination was seen to be large, and the results are not accurate; in the future it will be necessary to analize the influence of certain error sources to increase the system performance. Firstly, data was collected using a simple set-up, in an attempt to reproduce the procedures followed in the experiments done by Giaever and Keese (1986). In these measurements, serial load resistance was large (1 MΩ), to limit the current through the cell to 1 μA. Signal-to-Noise Ratio (SNR) was low due to the large noise contribution from high resistance values. Other, improved setups should be used in the future. Secondly, the proposed model has the advantage that it needs only one parameter (R_{gap}), in comparison with another reported model using three parameters (Giaever, 1991). This makes easy to handle experimental data, but also introduces inaccuracies. The possibility of adding more parameters to the model should be considered in the future. Finally, finite element simulations must be developed for different cell lines to really test the cell identity in biometric applications.

10. Acknowledgements

This work is in part supported by the funded Project: Auto-calibración y auto-test en circuitos analógicos, mixtos y de radio frecuencia: Andalusian Government project P0-TIC-5386, co-financed with the FEDER program. We would also like to thank Citoquimica Ultraestructural Group (BIO132) of the Cell Biology Department, Seville University, for its experimental help in conducting cell culture experiments, and Blanca Buzón for her support on finite element simulation.

11. References

Åberg, P., Nicander, I., Hansson, J., Geladi, P., Holmgren, U. and Ollmar, S. (2004). Skin Cancer Identification Using Multi-frequency Electrical Impedance: A Potential Screening Tool, *IEEE Transaction on Biomedical Engineering*. vol. 51, nº 12, pp: 2097-2102.

Ackmann, J. (1993). Complex Bioelectric Impedance Measurement System for the Frequency Range from 5Hz to 1MHz. *Annals of Biomedical Engineering*, Vol. 21, pp. 135-146.

Applied Biophysics. http://www.biophysics.com/.

Beach, R.D. et al, (2005). Towards a Miniature In Vivo Telemetry Monitoring System Dynamically Configurable as a Potentiostat or Galvanostat for Two- and Three-Electrode Biosensors, *IEEE Transaction on Instrumentation and Measurement*, vol. 54, nº 1, pp: 61-72.

Bagotzky, V.S., Vasilyev, Y.B., Weber, J. and Pirtskhalava, N.. (1970). Adsorption of anions on smooth platinum electrodes. *J. Electroanal. Chem. & Interfacial Electrochem.*, Elsevier sequoia A.A., Netherlands, 27: 31-46 (1970).

Blady, B. & Baldetorp, B.. (1996). Impedance spectra of tumour tissue in comparison with normal tissue; a possible clinical application for electrical impedance tomography. *Physiol. Meas*., vol. 17, suppl. 4A, pp. A105–A115.

Borkholder, D. A., (1998). Cell Based Biosensors Using Microelectrodes, *PhD Thesis*. Stanford.

Bockris, J.O'M. & Reddy, A.K.N.. (1970). Modern electrochemistry. *Plenum Press*, New York.

COMSOL, The use of the Conductive Media DC Application Mode for time-harmonic problems, solution 904, support knowledge base, from http://www.comsol.com.

De Boer, R.W. & van Oosterrom, A. (1978). Electrical properties of platinum electrodes: Impedance measurements and time domains analysis, *Med. Biol. Eng. Comput*., 16: 1-9.

DeRosa, J.F. & Beard, R.B.. (1977). Linear AC electrode polarization impedance at smooth noble metal interfaces, *IEEE Transactions on Biomedical Engineering,* BME-24(3): 260-268.

Giaever, I. et al. (1986). Use of Electric Fields to Monitor the Dynamical Aspect of Cell Behaviour in Tissue Cultures. *IEEE Transaction on Biomedical Engineering*, vol. BME-33, No. 2, pp. 242-247.

Giaever, I. & Keese, C. R. (1991). Micromotion of mammalian cells measured electrically, *Proc. Nail. Acad. Sci. USA. Cell Biology*, vol. 88, pp: 7896-7900, Sep. 1991.

Giebel, K.F. et al. (1999). Imaging of cell/substrate contacts of living cells with surface plasmon resonance microscopy, *Biophysics Journal*, vol. 76, pp: 509–516.

Grimnes, S. & Martinsen, O. (2008). Bio-impedance and Bioelectricity Basics, *Second edition. Academic Press*, Elsevier.

Huang X. et al. (2004). Simulation of Microelectrode Impedance Changes Due to Cell Growth, *IEEE Sensors Journal*, vol.4, nº5, pp: 576-583.

Joye N. et al. (2008). An Electrical Model of the Cell-Electrode Interface for High-density Microelectrode Arrays, *30th Annual International IEEE EMBS Conference*, pp: 559-562.

Linderholm, P., Braschler. T., Vannod, J., Barrandon, Y., Brouardb, M., and Renaud, P. (2006). Two-dimensional impedance imaging of cell migration and epithelial stratification. *Lab on a Chip*. 6, pp: 1155–1162.

Manickam, A., Chevalier, A., McDermott, M., Ellington, A. D. and Hassibi, A. (2010). A CMOS Electrochemical Impedance Spectroscopy (EIS) Biosensor Array, *IEEE Transactions on Biomedical Circuits and Systems*, vol 4, nº 6. pp: 379-390.

Olmo, A. & Yúfera, A. (2010). Computer Simulation of Microelectrode Based Bio-Impedance Measurements with COMSOL, *Third International Conference on Biomedical Electronics and Devices, BIODEVICES 2010*. pp: 178-182. Valencia, Spain.

Onaral, B. & Schwan, H.P. (1982). Linear and nonlinear properties of platinum electrode polarization. Part I: Frequency dependence at very low frequencies, *Med. Biol. Eng. Comput.*, 20: 299-306.

Onaral, B. & Schwan, H.P. (1983). Linear and nonlinear properties of platinum electrode polarization. Part II: time domain analysis, *Med. Biol. Eng. Comput.*, 21: 210-216.

Radke, S.M & Alocilja, E.C. (2004). Design and Fabrication of a Microimpedance Biosensor for Bacterial Detection, *IEEE Sensor Journal*, vol. 4, nº 4, pp: 434-440.

Robinson, D.A. (1968). The electrical properties of metal microelectrodes, *Proceedings of the IEEE*, 56(6): 1065-1071.

Schwan, H. P. (1957). Electrical properties of tissue and cell suspensions. *Advances in Biological and Medical Physics. New York, Academic press*, vol. 5, pp. 147–224.

Schwan, H.P. (1963), "Determination of biological impedance", in Physical in Biological Research, W.L. Nastuk, *Ed. New York: Academic press*, 6(ch.6) (1963).

Schwan, H.P. (1968). Electrode polarization Impedance and Measurement in Biological Materials, *Ann. N.Y. Acad. Sci.*, 148(1): 191-209.

Schwan, H.P. (1992). Linear and Nonlinear electrode polarization and biological materials, *Annal. Biomed. Eng.*, 20: 269-288.

Schwan, H.P. (1992), Linear and Nonlinear electrode polarization and biological materials, *Annal. Biomed. Eng.*, 20: 269-288.

Simpson, R.W., Berberian, J.G. and Schwan, H.P. (1963). Nonlinear AC and DC polarization of platinum electrodes, *IEEE Transactions on Biomedical Engineering*. BME-27(3): 166-171.

SpectreHDL Reference Manual, Cadence Design Systems Inc.

Yúfera, A. et al. (2005). A Tissue Impedance Measurement Chip for Myocardial Ischemia Detection, *IEEE Transaction on Circuits and Systems: Part I*. vol. 52, nº.12 pp: 2620-2628.

Yúfera A. & Rueda, A. (2010a). A Close-Loop Method for Bio-Impedance Measurement with Application to Four and Two-Electrode Sensor Systems, *Chapter 15 in New Developments in Biomedical Engineering, IN-TECH*, Edited by: Domenico Campolo, pp: 263-286.

Yúfera, A. & Rueda, A. (2010b). Design of a CMOS closed loop system with applications to bio-impedance measurements, *Microelectronics Journal*. Elsevier. vol. 41, pp: 231-239.

Yufera, A. & Rueda, A. (2011). A Real-Time Cell Culture Monitoring CMOS System Based on Bio-impedance Measurements. *Kluwer Academic Pub.: Analog Integrated Circuits and Signal Processing, Special Issue on ICECS 2009*. (Accepted for publication)

Wang, P & Liu, Q. editors (2010). Cell-Based Biosensors: Principles and Applications, Artech House Series.

Warburg, E. (1899). Ueber das verhalten sogenannter unpolarisirbarer elektroden gegen wechselstrom, *Physik & Chemie*, 3: 493-499.

Advanced Biometric Technologies

Edited by Dr. Girija Chetty

ISBN 978-953-307-487-0
Hard cover, 382 pages
Publisher InTech
Published online 09, August, 2011
Published in print edition August, 2011

The methods for human identity authentication based on biometrics â€“ the physiological and behavioural characteristics of a person have been evolving continuously and seen significant improvement in performance and robustness over the last few years. However, most of the systems reported perform well in controlled operating scenarios, and their performance deteriorates significantly under real world operating conditions, and far from satisfactory in terms of robustness and accuracy, vulnerability to fraud and forgery, and use of acceptable and appropriate authentication protocols. To address some challenges, and the requirements of new and emerging applications, and for seamless diffusion of biometrics in society, there is a need for development of novel paradigms and protocols, and improved algorithms and authentication techniques. This book volume on â€œAdvanced Biometric Technologiesâ€ is dedicated to the work being pursued by researchers around the world in this area, and includes some of the recent findings and their applications to address the challenges and emerging requirements for biometric based identity authentication systems. The book consists of 18 Chapters and is divided into four sections namely novel approaches, advanced algorithms, emerging applications and the multimodal fusion. The book was reviewed by editors Dr. Girija Chetty and Dr. Jucheng Yang We deeply appreciate the efforts of our guest editors: Dr. Norman Poh, Dr. Loris Nanni, Dr. Jianjiang Feng, Dr. Dongsun Park and Dr. Sook Yoon, as well as a number of anonymous reviewers.

How to reference

In order to correctly reference this scholarly work, feel free to copy and paste the following:

Alberto Yúfera, Alberto Olmo, Paula Daza and Daniel Cañete (2011). Cell Biometrics Based on Bio-Impedance Measurements, Advanced Biometric Technologies, Dr. Girija Chetty (Ed.), ISBN: 978-953-307-487-0, InTech, Available from: http://www.intechopen.com/books/advanced-biometric-technologies/cell-biometrics-based-on-bio-impedance-measurements

INTECH
open science | open minds

InTech Europe
University Campus STeP Ri
Slavka Krautzeka 83/A
51000 Rijeka, Croatia
Phone: +385 (51) 770 447
Fax: +385 (51) 686 166

InTech China
Unit 405, Office Block, Hotel Equatorial Shanghai
No.65, Yan An Road (West), Shanghai, 200040, China
中国上海市延安西路65号上海国际贵都大饭店办公楼405单元
Phone: +86-21-62489820
Fax: +86-21-62489821

www.intechopen.com

IntechOpen

IntechOpen